JCTC Journal of Chemical Theory and Computation

Article

pubs.acs.org/JCTC

Chemical Interactions and Spin Structure in $(O_2)_4$: Implications for the ε-O_2 Phase

M. A. García-Revilla,*[,†,⊥] E. Francisco,[‡] A. Martín Pendás,[‡] J. M. Recio,[‡] M. Bartolomei,[§] M. I. Hernández,[§] J. Campos-Martínez,[§] E. Carmona-Novillo,[§] and R. Hernández-Lamoneda[∥]

[†]Departamento de Química, División de Ciencias Naturales y Exactas, Universidad de Guanajuato, 36050-Guanajuato, México

[‡]Departamento de Química Física y Analítica, Facultad de Química, Universidad de Oviedo, 33006-Oviedo, Spain

[§]Instituto de Física Fundamental, Consejo Superior de Investigaciones Científicas (IFF-CSIC), Madrid, Spain

[∥]Centro de Investigaciones Químicas, Universidad Autónoma del Estado de Morelos, Mor, México

ABSTRACT: The chemical interactions and spin structure of $(O_2)_4$ in its ground singlet state are analyzed by means of Quantum Chemical Topology descriptors. The energetic contributions of the Interacting Quantum Atoms approach are used to obtain information about the class of interactions displayed along the dissociation path of $(O_2)_4$. The exchange-correlation contribution to the binding energy is non-negligible for the O_2−O_2 interactions at intermolecular distances close to those found for the pressure induced ε phase of solid (O_2) and this strengthening of the intermolecular bonding is built up from a simultaneous weakening of the intramolecular bond. This result is of interest in connection with the observed softening of the IR vibron frequency in the lower pressure range of the ε phase. The spin structure in the real space along the dissociation process is interpreted with the help of the so-called electron number distribution functions. At large distances, the four triplet O_2 molecules are arranged in a way consistent with an antiferromagnetic structure, whereas at short distances, a significant spin redistribution is driven by the exchange process and it involves a propensity toward a null magnetic moment per molecule. Such probability behavior can be related with the magnetic evolution of solid oxygen across the $\delta \rightarrow \varepsilon$ phase transition. Additional calculations of $(O_2)_4$ excited states support the conclusion that the relative stabilization and magnetic features of the ground singlet state are due to the onset of the new intermolecular bonds, and not to an exclusive modification of the electronic character within the O_2 molecules.

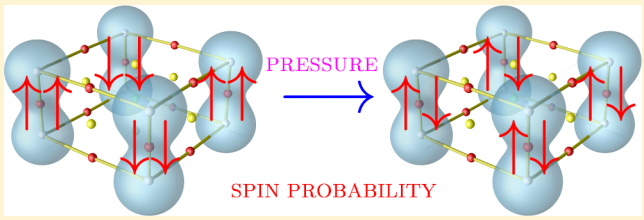

1. INTRODUCTION

Molecular systems constitute a perfect landscape for searching for exotic behavior of materials under extreme conditions. Here, exotic is employed in the sense of unexpected or novel, demanding state-of-the-art simulation techniques able to offer us a deep understanding of the new physics brought about by high pressure and/or high temperature. That is one of the reasons why the phase transitions occurring in oxygen under extreme pressure conditions have been intensively studied in the past three decades (see refs 1−6 and references therein).

At low temperatures and as pressure increases from zero, molecular oxygen displays four solid phases:[7,8] α, δ, ε, and ζ. Modifications in the magnetic behavior along the compression process evidence big differences in the spin structure of the solid oxygen phases when compared with the gas phase. Under room conditions, O_2 is a paramagnetic gas with molecules in $^3\Sigma_g^-$ electronic ground states. Magnetic interactions among these molecules become crucial in the α and δ phases, as they exhibit antiferromagnetic ordering.[9,10] In the pressure range near the δ−ε transition (8−11 GPa), spectroscopy records have shown strong modifications in the vibrational modes[11,12] and the low-energy electronic transitions,[9,13] suggesting that the transition to ε-O_2 might involve a magnetic collapse. The hypothesis was confirmed by Goncharenko,[14] with neutron diffraction data clearly showing that long-range magnetic ordering disappears at the phase transition. Other significant changes occur across the δ−ε transition: a volume collapse, the onset of strong infrared absorption, and a color change from orange to dark red. If the solid is subject to higher pressures, it turns to a black color, and then it transforms to the metallic ζ phase at about 96 GPa.

Although some nonmagnetic structures (such as the formation of O_4 singlet molecular units,[12] cyclic-O8 molecular units for dense oxygen,[15] or herringbone polymeric $(O_2)_n$ chains[16]) were proposed to be compatible with the available observations. Two independent X-ray experiments[2,3] definitively concluded in 2006 that the building block of the ε phase comprises a cluster of four oxygen molecules, $(O_2)_4$. These clusters, of rhomboid shape, arrange in layers with O_2 intramolecular axes nearly perpendicular to the layer plane. Along the δ−ε transition and as the solid is further compressed, important changes in the intermolecular O_2−O_2 distances are displayed, while the intramolecular O−O bond distance nearly keeps its gas phase value. Nevertheless, and interestingly, the pressure dependence of the infrared vibron

Received: December 6, 2012

   dx.doi.org/10.1021/ct301070f | J. Chem. Theory Comput. XXXX, XXX, XXX−XXX

frequency exhibits a minimum around 20 GPa, while the frequency of the Raman vibron increases monotonically with pressure.[12] All this information suggests that a weak chemical bond within $(O_2)_4$ is responsible for the changes of the physical properties along the compression process. The stability and spectroscopic behavior of this structure was also investigated using the available Density Functional Theory implementations, reaching no definitive conclusions.[16−18] This might be a consequence of the difficulties of the approximated functionals to describe weak intermolecular forces as well as the multiconfigurational character of molecular oxygen clusters in low-spin multiplicity states.

Recently, some of us obtained a reliable estimation of the intermolecular potential energy surface of the lowest singlet state of the molecular oxygen tetramer in a cuboid arrangement, with the centers of mass of the O_2 diatoms forming a square, by means of high level *ab initio* calculations.[19] In contrast with previous analyses, it was found that a multiconfigurational ansatz is unavoidable for such a system, and that $(O_2)_4$ should be considered as a van der Waals-like complex with an incipient chemical bonding progressively increasing as the cluster is compressed. On the basis of those *ab initio* calculations, we proposed a simple model consisting of a $(O_2)_4$ cluster embedded in a proper network of surrounding oxygen molecules, mimicking a layer of ε-O_2. In that scheme, the energy of the system was obtained as a sum of the internal (ab initio) energy of the $(O_2)_4$ complex plus intercluster interaction energies which where approximated as a sum of pairwise O_2-O_2 interactions. The model reproduced for the first time the experimental behavior[3] of the intra- and intercluster distances in the lower pressure range, indicating that an accurate treatment of the $(O_2)_4$ complex is a key element for the rationalization of the behavior of this phase of oxygen. It is worth noting that the importance of the $(O_2)_4$ unit in ε-O_2 previously stood out in a joint experimental/computational study of inelastic X-ray scattering in ε-O_2,[6] although it is also indicated that interactions between $(O_2)_4$ units become more important in the higher pressure range.

Following the conclusions outlined above, and since a complete "bulk" study of the solid by means of *ab initio* calculations is nowadays impossible, we believe that an exhaustive analysis of the chemical interactions in $(O_2)_4$ would provide a deeper understanding of the origin of the physical changes that occur across the $\delta-\varepsilon$ phase transition, including spectroscopic and magnetic behavior. Given that the use of correlated levels of theory has been found to be essential in this system,[19] and recognizing that no standard method provides chemical bonding information for correlated wave functions, we have decided to tackle this problem using recently proposed real space formalisms,[20−26] invariant under orbital transformations and equally applicable to correlated and noncorrelated descriptions. The electronic structure analysis of the correlated wave functions, obtained from the dissociation of the molecular oxygen tetramer, is fundamental for the characterization of the intra- and intermolecular interactions in the ε phase.

Our aim in this paper is two-fold. First, we try to provide a full characterization of the chemical interactions in singlet $(O_2)_4$ using *ab initio* tools within the framework of Real Space Theories (RSTs) of chemical bonding. Second, we intend to obtain some insight into the microscopic origin of the magnetic collapse observed at the $\delta \rightarrow \varepsilon$ transition through an analysis of the spin structure of different geometries of the molecular oxygen tetramer. The study is supplemented by calculations of excited electronic states to investigate the possible role of nonadiabatic interactions in the formation of the new bonds within the cluster.

The paper is organized as follows. In the next section, we will present the basic theoretical tools from real space treatments of chemical bonding, as well as a very brief introduction to the electron number distribution functions (EDFs). In section 3, we will comment on the computational details of our calculations. Section 4 will present and discuss our results, first regarding the nature of the chemical interactions found in the molecular oxygen tetramer and then passing to our microscopic image of the magnetic collapse. Finally, some conclusions and future prospects will be highlighted.

2. THEORETICAL BACKGROUND

Chemical Interactions from Quantum Chemical Topology. RSTs[20−26] provide an orbital invariant alternative to the prevalent molecular orbital paradigm that has dominated the field for more than 50 years. In such approaches, the wave function of a system is analyzed in real, not Fock space, and bonding indices are obtained through integrals of chemically relevant fields constructed from reduced density matrices over well-defined regions in $\mathcal{R}^3$. Among the most used RSTs, we find the Quantum Theory of Atoms in Molecules (QTAIM), developed by Bader and co-workers,[20] where the physical space is partitioned exhaustively into quantum atoms defined as the attractor basins of the gradient vector field of the electron density, ρ. This field also defines the molecular graph through particular flux lines joining atomic nuclei, known as bond paths. The atoms of the QTAIM are separated by interatomic surfaces which fulfill the zero flux condition:

$$\nabla\rho(\mathbf{r})\cdot\hat{\mathbf{n}} = \mathbf{0} \tag{1}$$

where $\hat{\mathbf{n}}$ is the exterior normal unit vector to the interatomic surface. The bond paths, which link the so-called bond critical points (BCP) of ρ with the nuclei,[27−38] have been usually put in a one to one correspondence with the chemically intuitive concept of chemical bond.

Many local descriptors computed at BCPs have been devised to extract chemical information from the electron density. For instance, the ellipticity $\bar{\varepsilon}$ is used to measure the deviation of a given bond from cylindrical symmetry and has been related to the π character in simple unsaturated hydrocarbons.[39] π-like interactions are fundamental in the description of the chemical bond of the oxygen molecule and should be analyzed in the chemical interactions of the molecular oxygen tetramer. Ellipticity is defined as the ratio of two curvatures at the BCPs; the curvatures used for $\bar{\varepsilon}$ are those of a plane perpendicular to the bond path at the BCP

$$\bar{\varepsilon} = \frac{\lambda_1}{\lambda_2} - 1 \tag{2}$$

where λ_i is the eigenvalue of the curvature and $|\lambda_1| > |\lambda_2|$. Another topological descriptor of the chemical bond is the Laplacian of the electron density calculated at the BCP

$$\nabla^2\rho(\mathbf{r})_{\mathrm{bcp}} = \nabla\cdot\nabla\rho(\mathbf{r})_{\mathrm{bcp}} \tag{3}$$

Negative (positive) values of the laplacian at the BCP signal local density concentrations (depletions) and have thus been interpreted as a measure of shared (closed) shell interactions.[20]

The local interpretation of the chemical bond has however generated an interesting controversy related to the true meaning of bond paths in the QTAIM,[27−38] which is starting to fade

dx.doi.org/10.1021/ct301070f | J. Chem. Theory Comput. XXXX, XXX, XXX−XXX

thanks to new developments in RSTs, where a new view of the topology of the chemical interactions is presented that agrees with the traditional models of chemical bonding.

These new developments have shown that the use of integrated, global descriptors in the QTAIM provides far more stable results that overcome many of the above-mentioned criticisms.[37,38,40] One of these global topological descriptors is the electron delocalization index (DI), a measure of bond order in real space that describes the number of electron pairs delocalized between two regions in space. The DI is defined through the following expression[41,42] (note that atomic units are used throughout this work except as otherwise stated)

$$\mathrm{DI} = \delta^{AB} = -2 \int_{\Omega_A} \mathrm{d}\mathbf{r}_1 \int_{\Omega_B} \mathrm{d}\mathbf{r}_2\, \rho_2^{\mathrm{xc}}(\mathbf{r}_1, \mathbf{r}_2) \tag{4}$$

Here, $\rho_2^{\mathrm{xc}}(\mathbf{r}_1,\mathbf{r}_2)$ is the exchange-correlation density, or the irreducible part of the standard pair density, $\rho_2(\mathbf{r}_1,\mathbf{r}_2)$, and Ω_A and Ω_B are partitions of the real space such that $\cup_i^m \Omega_i = \mathcal{R}^3$ and $\Omega_i \cap \Omega_j = \varnothing$. It takes into account all the two-particle correlations that cannot be expressed in terms of lower order density matrices, in this case, the electron density. Thus,

$$\rho_2(\mathbf{r}_1, \mathbf{r}_2) = \rho(\mathbf{r}_1)\, \rho(\mathbf{r}_2) + \rho_2^{\mathrm{xc}}(\mathbf{r}_1, \mathbf{r}_2) \tag{5}$$

In the case of single determinant wave functions, $\rho_2^{\mathrm{xc}}(\mathbf{r}_1,\mathbf{r}_2)$ can be defined in terms of the nondiagonal first order density matrix:

$$\begin{aligned} \rho_2^{\mathrm{xc}}(\mathbf{r}_1, \mathbf{r}_2) &= \rho_1(\mathbf{r}_1; \mathbf{r}_2)\, \rho_1(\mathbf{r}_2; \mathbf{r}_1), \\ &= \sum_{i,j} \phi_i(\mathbf{r}_1)\, \phi_j(\mathbf{r}_1)\, \phi_i(\mathbf{r}_2)\, \phi_j(\mathbf{r}_2) \end{aligned} \tag{6}$$

so the 6D integrals required to obtain the DIs may be easily simplified to products of 3D ones. Actually, the DI in this case acquires the following form in terms of domain-restricted overlap integrals, $\delta^{AB} = 2\sum_{i,j} S_{ij}^A S_{ij}^B$. For multideterminant (MD) wave functions,

$$\rho_2^{\mathrm{MD}}(\mathbf{r}_1, \mathbf{r}_2) = \sum_{ijkl} c_{ijkl}\, \phi_i(\mathbf{r}_1)\, \phi_j(\mathbf{r}_1)\, \phi_k(\mathbf{r}_2)\, \phi_l(\mathbf{r}_2) \tag{7}$$

where the c_{ijkl} are provided by the particular level of theory employed. In this study, delocalization indices from Configuration Interaction (CI) and Complete Active Space Self Consistent Field (CASSCF) correlated wave functions were computed thanks to efficient algorithms developed by some of us.[43] DIs not only provide quantitative measures of electron delocalization but have also proven valuable in classifying chemical interactions. We have recently shown,[38] for instance, that the sigmoid or exponential decay of DIs with internuclear distance is related to the bonding or nonbonding character, respectively, of a given interaction. Note that when $A = B$ we are computing the localization index, λ^A, instead. The values of δ^{AB} (λ^A) are dimensionless, but they are interpreted as electron paris that are delocalized (localized) between atoms (in an atom).

In a similar fashion, now in the energetic realm, our Interacting Quantum Atoms (IQA) approach[44−46] emerges as a physically meaningful tool to study chemical interactions. IQA starts by noticing that the total energy of a system can be exactly written in terms of the first and second order density matrices. For a given partition of the real space in a set of Ω_i domains, the total energy turns out to be a sum of intra- and interdomain contributions:

$$E = \sum_A \int_{\Omega_A} \mathrm{d}\mathbf{r}_1 \left(\hat{T} - \sum_B \frac{Z_B}{r_{1B}} \right) \rho_1(\mathbf{r}_1; \mathbf{r}_{1'}) + \sum_{A>B} \frac{Z_A Z_B}{R_{AB}} + \frac{1}{2} \sum_{A,B} \int_{\Omega_A} \mathrm{d}\mathbf{r}_1 \int_{\Omega_B} \mathrm{d}\mathbf{r}_2\, \frac{\rho_2(\mathbf{r}_1, \mathbf{r}_2)}{r_{12}} \tag{8}$$

where $\rho_1(\mathbf{r}_1;\mathbf{r}_{1'})$ and $\rho_2(\mathbf{r}_1,\mathbf{r}_2)$ are the first-order nondiagonal and the second-order diagonal reduced density matrices, respectively. So, the total energy of a system can be written as the sum of atomic self-energies, E_{self}^A, and pair interaction potential energies, E_{int}^{AB}:

$$E = \sum_A E_{\mathrm{self}}^A + \sum_{A>B} E_{\mathrm{int}}^{AB} \tag{9}$$

$$E_{\mathrm{self}}^A = T^A + V_{\mathrm{ee}}^{AA} + V_{\mathrm{en}}^{AA} \tag{10}$$

$$E_{\mathrm{int}}^{AB} = V_{\mathrm{ne}}^{AB} + V_{\mathrm{en}}^{AB} + V_{\mathrm{nn}}^{AB} + V_{\mathrm{ee}}^{AB} \tag{11}$$

Although IQA is usually employed in the QTAIM framework, its density matrix partitioning[47] is easily generalized[44] to other atomic definitions, fuzzy or not, such as those of Becke[24] or Hirshfeld.[25] IQA may be equally used for single- and multideterminant wave functions, thus providing a completely general tool for examining chemical interactions. The power of IQA over other methodologies lies in how easily it is able to isolate all chemically intuitive energetic terms. Molecular binding energies, for instance, are immediately obtained by subtracting appropriate group or atomic reference energies, usually *in vacuo*:

$$E_{\mathrm{bind}} = E - \sum_A E_{\mathrm{vac}}^A \tag{12}$$

Substituting the total energy, eq 9, in the last equation and defining the atomic (or group) deformation energy as

$$E_{\mathrm{def}}^A = E_{\mathrm{self}}^A - E_{\mathrm{vac}}^A \tag{13}$$

the binding energy turns out to be a sum of atomic (group) deformation energies and pair interaction contributions:

$$E_{\mathrm{bind}} = \sum_A E_{\mathrm{def}}^A + \frac{1}{2} \sum_{A,B\neq A} E_{\mathrm{int}}^{AB} \tag{14}$$

Similarly, using eq 5 the interaction energy can be written as

$$E_{\mathrm{int}}^{AB} = V_{\mathrm{cl}}^{AB} + V_{\mathrm{xc}}^{AB} \tag{15}$$

where V_{cl}^{AB} and V_{xc}^{AB} are the classical and exchange-correlation contributions, respectively. The former is defined as the sum of Coulombic nucleus−electron and nucleus−nucleus interactions plus the pure Coulombic electron−electron interaction, i.e., $V_{\mathrm{ne}}^A + V_{\mathrm{en}}^{AB} + V_{\mathrm{nn}}^{AB} + \int_{\Omega_A} \mathrm{d}\mathbf{r}_1 \int_{\Omega_B} \mathrm{d}\mathbf{r}_2\, \rho(\mathbf{r}_1)\, \rho(\mathbf{r}_2) r_{12}^{-1}$, see eq 11. The exchange-correlation contribution is defined by $\int_{\Omega_A} \mathrm{d}\mathbf{r}_1 \int_{\Omega_B} \mathrm{d}\mathbf{r}_2\, \rho_2^{\mathrm{xc}}(\mathbf{r}_1,\mathbf{r}_2)\, r_{12}^{-1}$, the pure exchage-correlation interaction part of the V_{ee}^{AB} term of eq 11. Gathering the interaction terms in this peculiar way is again chemically meaningful, for the classical and exchange-correlation terms are immediately associated with the ionic and covalent contributions to the bond energy. In this way, IQA transforms each interatomic interaction into three chemically appealing energetic objects: deformation (promotion), ionicity, and covalency.

As of today, IQA has been used to shed light in a number of interesting chemical bonding problems, e.g., the nature of the hydrogen bond,[48] the real space origin of rotation barriers and other stereoelectronic effects,[49] the relative role of donation and

dx.doi.org/10.1021/ct301070f | J. Chem. Theory Comput. XXXX, XXX, XXX−XXX

back-donation in transition metal complexes,[50] et cetera. Furthermore, it has become clear that both terms in eq 15 are independent, so that ionicity and covalency are not mutually exclusive, as usually thought, but two different dimensions in chemical bonding that may evolve differently. We will use in this work QTAIM based IQA quantities, together with DIs to examine the chemical interactions in the molecular oxygen tetramer.

Electron Number Distribution Functions. Further information on chemical bonding from real space partitioning may be obtained by examining the statistics of electron count in different domains. Some of us are actively working in developing such statistical models of the chemical bond.[51−56] The basic object in such new models is the so-called electron number distribution functions (EDF). EDFs are the probabilities of finding a total number of electrons, N, in a given integer distribution of electrons, $S \equiv \{n_1,n_2,...,n_m\}$, in which there are n_1 electrons in Ω_1, n_2 in Ω_2, and n_m in Ω_m, and $N = n_1 + ... + n_m$. For a partition of $\mathcal{R}^3$ as given before and when using QTAIM domains, Ω_i corresponds to different basins and S is named as a real space resonance structure (RSRS). Such probability is given by the following expression:

$$p(S) = \frac{N!}{n_1!...n_m!}\int_D |\psi|^2 \, d\mathbf{r}_1...d\mathbf{r}_N \tag{16}$$

where D is a $3N$-dimensional domain such that we integrate the first n_1 electrons in Ω_1, the second n_2 electrons in Ω_2, and so on. Clearly, the set of all the possible probabilities $p(S)$, the EDFs, fulfills probability sum rule $\sum_S p(S) = 1$. EDFs may be also spin-resolved, so we may compute probabilities of finding particular sets of spins in different basins. For this purpose, the integration must be done in each basin through spin coordinates. Moreover, it is possible to define partial EDFs, where $\cup_i\Omega_i \subset \mathcal{R}^3$ ($\sum_i n_i \leq N$), by adding a complementary region $\mathcal{R}^3-\cup_i\Omega_i$ containing the $N-\sum_i n_i$ remaining electrons.[51] This is particularly important in the present study, for there are not so many quantities that may describe the spatial spin arrangement of electrons, particularly in singlets (notice that the spin density of a closed-shell singlet vanishes everywhere). With the help of EDFs, simple models of bonds long known to chemists (the two-center, two-electron bond; the three-center, two-electron bond; etc.) may be immediately developed and explained in terms of more or less heavily modified independent particle events.

It is also worthy to mention that obviously all these descriptors and probabilities change with the level of theory used in the electronic calculation or, in other words, with the electronic correlation that in simple terms made the electrons behave as particles depending on each other and hence changing the probabilistic behavior in different regions of space.

3. COMPUTATION DETAILS

In this work, we model the compression or dissociation process in the same way as in a previous study,[19] as the concerted stretching of intermolecular distances in a symmetry-restricted $(O_2)_4$ cluster of cuboid D_{4h} shape, both in its fundamental and low-lying excited singlet states. It has been experimentally determined that the $(O_2)_4$ unit has a rhomboid shape[2,3] with nearly right angles, so it can be approximated by a cuboid. Hence, we have considered the geometry of higher symmetry in order to reduce computational time. Thus, the centers of mass of the respective O_2 molecules form a square whose side d is varied between 1.5 and 4.5 Å, maintaining the intramolecular O−O distance fixed at 1.2065 Å.[57] Experimental studies report no changes in the intramolecular distance along the compression process.[2] The wave functions and interaction energies were obtained at the CASSCF[8,8]/aug-cc-pVQZ level of theory, since IQA needs a well-defined two-particle density that is unfortunately not available at higher levels of theory. The complete active space is defined by distributing eight electrons in eight molecular orbitals correlating asymptotically with the $\pi_g^\star$ shell of four O_2 molecules. The counterpoise method[58,59] was applied to correct for the basis set superposition error. The estimated BSSE correction for the CASSCF(8,8)/aug-cc-pVQZ theory level in the present work is of about 10 meV.

In order to analyze the possible effect of excited states on the ground potential specifically in the repulsive region, we performed state-average calculations of the lowest 14 singlet states of A_g symmetry with equal weights for each state. The active space was the same as mentioned above. Test calculations were also made to check the stability of the results with respect to (a) the size of the active space and (b) inclusion of dynamic electron correlation. In the first case, we increased the active space to 24 valence electrons distributed in 16 molecular orbitals correlating with the O_2 π_g and π_u molecular orbitals. In the second case, we performed complete active space second order perturbation theory (CASPT2) calculations on the four lowest lying singlet states using as a reference the smaller active space mentioned above. All calculations used the program MOLPRO.[60]

Energetic profiles and wave functions were obtained with the GAMESS-US and MOLPRO programs.[61,60] DI (δ) and localization indexes (λ), V_{cl}, and V_{xc} were calculated along the energetic profiles using a recent implementation of the PROMOLDEN code.[62] EDFs were calculated along the potential energy surface using our EDF code.[54] The QTAIM descriptors were obtained with the AIMPAC software.[63]

4. RESULTS AND DISCUSSION

Interaction Energies. The CASSCF interaction energy (V) profile of the singlet ground state of the molecular oxygen tetramer is shown in Figure 1 (upper panel) as a function of the length (d) of the square side formed by the four oxygen molecules. This supermolecular calculation is compared in the same figure with an estimation of energy based on the assumption of additive pairwise contributions. In this approach, a linear combination of pairwise O_2-O_2 interactions, compatible with the lowest singlet state, has been built. The pairwise interaction energies have been computed at the same level of theory as the $(O_2)_4$ calculations (CASSCF). Many-body interaction energies (differences between supermolecular and pairwise calculations) are shown in the lower panel of Figure 1. As it can be observed, this approximation works very well for large intermolecular distances d; however, a significant many-body effect can be noticed for $d \lesssim 2.5$ Å, making the supermolecular repulsive wall much softer than in the case of a pure additive interaction. As discussed elsewhere,[19] the softening of the repulsive wall is a key element to explain the observed behavior of the intermolecular distances in ε-O_2 at low pressures. For the sake of comparison, we also show in Figure 1 analogous supermolecular and pairwise interaction energies obtained in ref 19 from a combination of CASPT2 and partially Restricted Coupled Cluster Singles and Doubles with Triples corrections (RCCSD(T)) calculations, labeled here as CC-PT2 for brevity (see ref 19 for details). It can be seen that, at this higher level of the theory, this many-body effect starts at larger intermolecular

dx.doi.org/10.1021/ct301070f | J. Chem. Theory Comput. XXXX, XXX, XXX−XXX

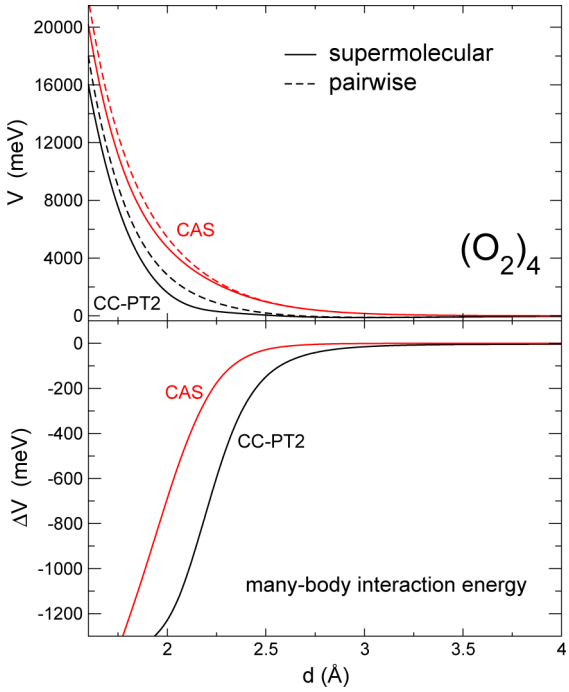

Figure 1. Upper panel: Interaction energies V with respect to the length of the side d of the square formed by the four oxygen molecules of the molecular oxygen tetramer in its ground singlet state as obtained from (i) supermolecular CASSCF calculations (red solid line) and (ii) a direct sum of pure O_2−O_2 interactions (red dashed line). Lower panel: Many-body interaction energy, $\Delta V(d)$, i.e., the difference between the supermolecular and the pairwise energies (in red). Higher level calculations of ref 19 (labeled as CC-PT2 and shown in black) are also depicted for comparison. A significant many-body effect making the repulsive wall softer is noticeable at both levels of theory.

distances d as the oxygen molecules come together. From this comparison we can expect that, although the dynamical correlation (attained by the higher level calculation) is needed for a quantitative description of the interaction energies, the essential features about the nature of the interaction can be studied at the CASSCF level. Analyses as those reported below, but carried out at higher levels of theory, would probably give modifications in the features of the interaction at intermolecular distances d larger than those obtained at the present CASSCF level of theory.

To explain this stabilization of the singlet interaction energy at small intermolecular distances d, one might wonder about the existence of couplings and avoided crossings with states asymptotically correlating to excited states of O_2. Indeed, the two lower lying excited states of O_2 are singlets ($^1\Delta_g$ and $^1\Sigma_g^+$), and at the shortest distances and along the repulsive wall, it could be possible that the monomers of ground singlet $(O_2)_4$ borrow character from these singlet excited states. Besides, the suggestion is appealing given the observed magnetic collapse at the boundary of the ε phase.[14] To check this hypothesis, we have performed state-average CASSCF calculations of the first 14 totally symmetric singlet (^1A_g) states of $(O_2)_4$, and the resulting interaction energies are displayed in Figure 2. Around 2 Å, the softening of the repulsive wall of the ground state curve can be noticed as compared with the slopes of the excited state. More importantly, no avoided crossings with the excited states are found. In order to test the lack of avoided crossings at higher levels of theory, we performed two separate test calculations. First, we increased the active space in the state average

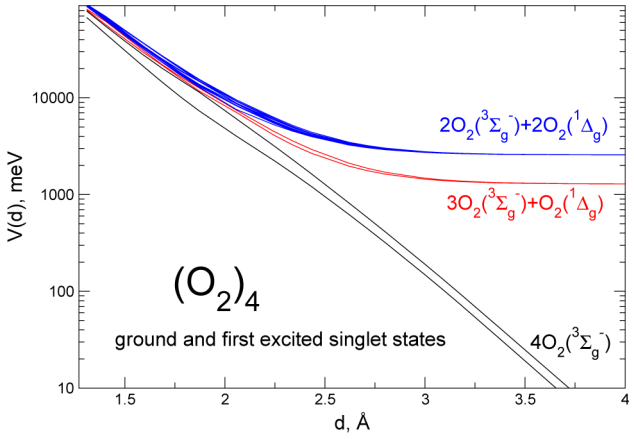

Figure 2. CASSCF state-averaged interaction energies for the first 14 singlet (A_g) states of the molecular oxygen tetramer. The first two states asymptotically correlate with four $O_2(^3\Sigma_g^-)$ (note that the zero of the energies has been set to this limit). Correlation with other excited states of the fragments is also indicated. It is noteworthy to stress that avoided crossings between the ground and any of the excited states are absent.

calculations to CAS(24,16), and second we performed multi-reference second order perturbation theory calculations on the four lowest singlet states using the smaller CAS(8,8) space. In both cases, the lack of avoided crossings with excited states remains true.

More details on the features of the electronic ground state can be obtained from inspection of the CI vector associated with each CASSCF calculation. We have interestingly found that along the molecular oxygen tetramer compression process the system is progressively losing its multireference character: in fact, the coefficient of the dominant determinant (that with the four lowest active orbitals fully occupied) is progressively increasing from 0.14, at 4.5 Å, to 0.97, at distances around 1.5 Å. Moreover, in the relevant experimental range of 2.0−2.2 Å, this coefficient is about 0.5−0.6. This result is consistent with the picture already given by some of the authors in ref 19, and it can be helpful to assess the correct approaches to be used to model the phase behavior at very high pressure.

Chemical Interactions from IQA. Figure 3 shows some local QTAIM descriptors at the bond critical points (BCP) together with relevant IQA contributions to bonding energies, V_{cl} and V_{xc}, all of them computed at d = 2.34 Å, corresponding to the geometry of the molecular oxygen tetramer in the ε phase at 11.4 GPa.[19] The molecular graph displays one intramolecular bond path (BP) per oxygen molecule and eight intermolecular BPs linking oxygen atoms belonging to neighboring monomers located in the molecular oxygen tetramer plane; i.e., every oxygen atom is linked through a BP with its nearest and next-nearest neighbors. The presence of bond paths speaks by itself of a preferred exchange channel,[37] although not everyone would be willing to call it a chemical bond. Further IQA descriptors help clarify the situation. For instance, the value of the electron density at the intermolecular BCPs, ρ_{bcp} = 0.025 au, is too small to be accepted as a standard O−O covalent bond, at clear variance with the intramolecular BCPs that show a 20 times larger value of ρ_{bcp} = 0.56 au. The topology of ρ shows, in addition, the presence of six ring critical points and one cage critical point, which all together configure the simplest possible critical points arrangement for a topological cube. The value of the ellipticity at the intermolecular BCPs, $\bar{\varepsilon}$ = 0.051, is much larger than that found for the intramolecular O−O bond, $\bar{\varepsilon}$ =

dx.doi.org/10.1021/ct301070f | J. Chem. Theory Comput. XXXX, XXX, XXX−XXX

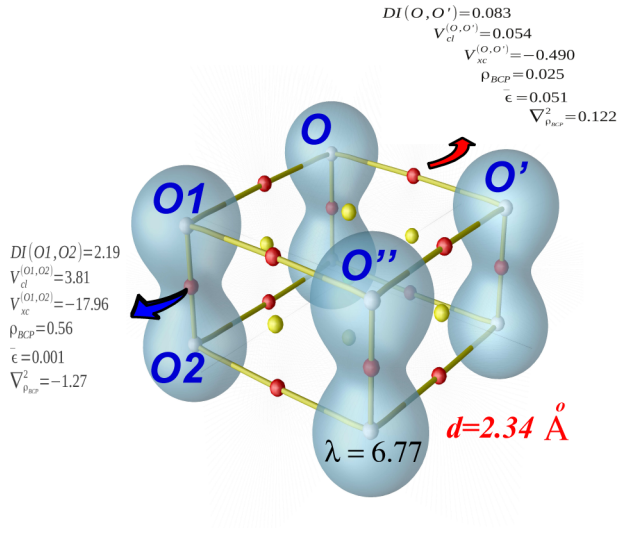

Figure 3. QTAIM-IQA topological descriptors for $(O_2)_4$. The blue envelope enclosing each oxygen molecule is an isosurface of the electron density, ρ = 0.35 au for for an easier sight. Color code: white balls, nuclear positions; red balls, bond critical points; yellow balls, ring critical points. There is a cage critical point in the middle of the cluster; it is not visible because of the view. Interaction energies, V_{xc} and V_{cl}, are given in eV, other quantities in au.

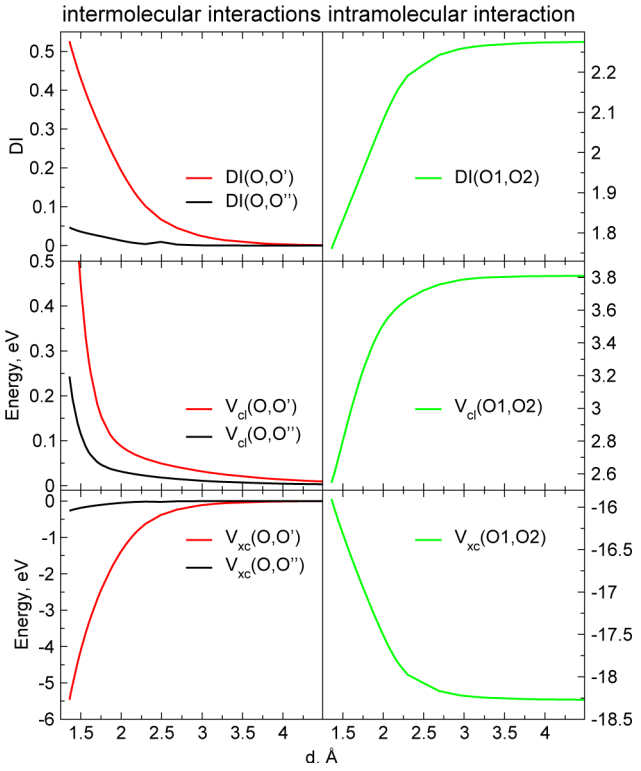

Figure 4. Evolution of IQA descriptors along the dissociation process for $(O_2)_4$. Rows label descriptors (first, DI; second, V_{cl}; third, V_{xc}), and columns label O−O pairs (left, intermolecular; right, intramolecular).

0.001. Such large ellipticities reveal the important contribution of the lone electron pairs of the oxygen atoms to their intermolecular interaction. Similarly, the value of the Laplacian at the BCP, $\nabla^2\rho(\mathbf{r})_{bcp}$, shows a local concentration of charge for the intramolecular O−O interaction, where $\nabla^2\rho(\mathbf{r})_{bcp} = -1.27$ au, thus a shared shell interaction that is usually identified in the QTAIM with a covalent bond. Contrarily, a depletion of charge for the intermolecular BCP is found, with $\nabla^2\rho(\mathbf{r})_{bcp} = 0.122$ au, a small positive value related to a weak and closed shell interaction.

Furthermore, the intramolecular delocalization index, DI(O1,O2) = 2.19, is characteristic of a double bond but is smaller than that computed for a free oxygen molecule at this level of theory, DI(O1,O2) = 2.3. This means (see below) that the O−O intramolecular bond is weakening upon complexation. Consequently, a non-negligible intermolecular delocalization is found, DI(O,O′) = 0.083, showing that, however weak, a distinct intermolecular interaction is present in this configuration. The building of a somewhat strong intermolecular interaction is more clearly noticed at smaller intermolecular distances, as discussed below. Note that the distance d = 2.34 Å, considered in Figure 3, corresponds to the lowest pressure boundary of the ϵ phase and that, as pressure increases, typical intermolecular distances d decrease to values around d = 2.0−2.2 Å.[3]

A more detailed picture of some of the magnitudes previously discussed as well as the processes taken place during compression is given in Figure 4. In the case of the intermolecular O−O interaction, the V_{cl} component decreases monotonically as d increases. It should be noticed here that it is possible to prove that the sum of all the classical interactions for two equivalent, neutral regions that do not overlap each other must be necessarily positive, i.e. destabilizing. The monotonic increase of this barrier upon compression is an indication of the classical instability of a neutral system of charges, which increases as they get closer and closer. It is interesting to observe that this destabilization is built from a corresponding decrease in the intramolecular value of V_{cl} (on the right part of the figure). This effect occurs by transferring charge density from the intramolecular bonding region, the region of MO overlapping in orbital terms, to the intermolecular nonbonding region, where MOs do not overlap significantly, as we compress the cluster.

Both the exchange-correlation contribution, V_{xc}, and the delocalization index display the expected behavior for the intermolecular interaction between the closest monomers. The DI exponentially decreases from 0.53 at d = 1.5 Å, asymptotically approaching zero at large distances. V_{xc} displays complementary behavior to DI, and this contribution (which is always stabilizing) decreases in absolute value as d increases, thus destabilizing the intermolecular interaction upon dissociation. For the shortest distances, relatively high absolute values of these descriptors clearly indicate the formation of a new intermolecular bond. Such DI values can be compared with the DI displayed at similar distances for systems with a clear bonding (nonbonding) character.[38] For instance, the bonded singlet H_2 has a DI value of 0.87 at the equilibrium geometry and displays a DI of 0.5 at distances of d = 1.5 Å, at variance with the DI value of 0.15 displayed at d = 1.5 Å for the nonbonded triplet of H_2. However, it must be pointed out that the compression process has not reached the regime where a new covalent interaction may be said to have been unambigously formed. As previously reported,[38] a sigmoidal shape of the DI curve would constitute a definitive signature of covalent bonding, but in the present study there is not yet a hint of an inflection point in the DI versus distance curves.

Interestingly, Figure 4 clearly shows that the increasing intermolecular interactions observed upon compression are built from a concomitant weakening of the O−O intramolecular bond. This peculiar behavior (irrespective of the fixed O−O intramolecular distance considered in the present analysis) can be at the core of the anomalous behavior of the IR vibron frequency as

dx.doi.org/10.1021/ct301070f | J. Chem. Theory Comput. XXXX, XXX, XXX−XXX

a function of pressure, which decreases after the $\delta-\varepsilon$ transition until reaching a minimum around 20 GPa.[12] This would also suggest that we are observing the early stages of the breaking of the O_2 double bond which eventually could lead to polymeric phases at pressures reaching the megabar regime.

Real space analyses are obviously compatible with traditional molecular orbital descriptions. In order to show it, we depict in Figure 5 the shapes of the four bonding HOMO natural orbitals

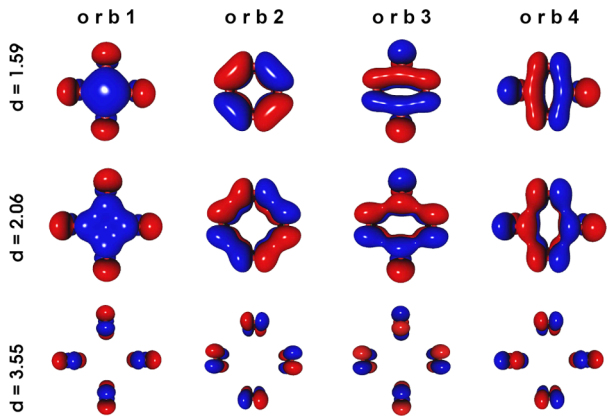

Figure 5. Evolution of the four HOMOs of the molecular oxygen tetramer in the ground singlet state for three intermolecular distances (in Å) obtained at the CASSCF level of theory. Occupation numbers are (1.025, 1.025, 1.019, 1.019), (1.636, 1.633, 1.556, 1.556), and (1.938, 1.923, 1.910, 1.910) at d = 3.55, 2.06, and 1.59 Å, respectively. This suggests a transition from orbital semioccupation at large intermolecular distances to double occupation at the smallest intermolecular distances d. All the MO surfaces correspond to a isocontour value of |0.05|.

at three different values of d. At the largest distance ($d \approx 3.5$ Å), the $\pi_g^\star$-type orbitals are rather localized around the skeletons of the diatomics, in accordance with a very weak intermolecular interaction. Their occupation numbers are close to 1, as well as those of the four HOMO antibonding orbitals (not shown) which at this distance are nearly degenerate. At shorter distances, the occupation of the latter tends to zero while that of the HOMO bonding ones progressively tends to a value near 2, and their shapes suggest covalent bonding. It is convenient to mention that the shapes of the orbitals at $d \approx 1.6$ Å are very similar to those reported in ref 64. However, note that at the typical cluster distances in the ε phase ($d \approx 2.0-2.2$ Å), an intermediate behavior of the HOMO bonding orbitals is found with occupation numbers of about 1.5 (middle panel of Figure 5), which confirms a weaker interaction between the O_2 molecules and supports the IQA description given above.

Chemical Interactions from EDFs. Richer information about charge transfer and chemical bonding may be obtained through EDFs. Notice that any population analysis, either in Fock or in real space, will give a zero net charge for any of the oxygen atoms in our D_{4h} symmetric molecular oxygen tetramer. This situation resembles the vanishing of the spin density in singlet wave functions. Fortunately, charge exchange, as well as spin exchange, may be easily followed from the EDF point of view. We have computed the probabilities of finding our eight active electrons placed in any possible arrangement of the four O_2 fragments that constitute the molecular oxygen tetramer. Figure 6 summarizes the results. We show the probability of finding a given integer number of (active) electrons {0, 1, 2, 3, 4, 5, 6, 7, 8} in any of the oxygen molecules, with no restrictions in the distribution of electrons for the rest of the system. At small

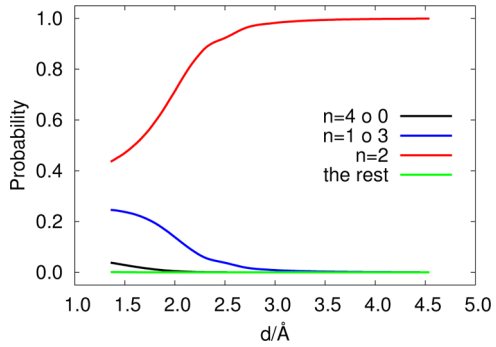

Figure 6. Spinless EDFs or the probability of finding a number n of active electrons in one oxygen molecule of the molecular oxygen tetramer, as a function of the length d (in Å).

distances, the relevant casuistry is 3-fold: (i) the oxygen molecule is neutral, n = 2, which is the most probable outcome; (ii) the oxygen molecule is transferring (receiving) one electron to (from) the rest of the system with n = 1 (n = 3); (iii) the oxygen molecule is transferring (receiving) two electrons to (from) the rest of the system, with n = 4 (n = 0). The other RSRSs have a negligible probability along the compression path, d. Data in Figure 6 show that for d sizes smaller than 2.5 Å, approximately, a distinctive chemical interaction appears that becomes increasingly important as the molecular oxygen tetramer is compressed. These findings agree with IQA results of the previous section. The equality of the probabilities of electron donation and acceptance implies a symmetric exchange of electrons, which corresponds, in our statistical modeling of chemical bonds,[51−55] to the onset of a covalent interaction. For instance, within a Hartree−Fock description of the H_2 molecule, the probability of a symmetric exchange of one electron is exactly equal to 0.25, this being interpreted as a single bond. In the present case, the analysis is complicated by the existence of various (intra- and intermolecular) bonds with the possibility of multiple exchanges. Finally, note that symmetric exchanges discussed here could not be captured from pure charge density analyses, which do not in principle alter the average electron distribution.

Spin Structure from EDF. The considerable electron exchange observed as we compress the molecular oxygen tetramer also points toward an accompanying change in the spin structure of the electron count statistics, and thus on the experimentally observed magnetic behavior. As we will see, our calculations show compelling evidence that the magnetic collapse occurring across the phase transition may be explained as a process localized within each of the $(O_2)_4$ units that would conform the ε phase. To that end, we are going to follow the spin-resolved EDFs along the compression (or dissociation) process.

Figure 7a shows the probability of finding spin projected $M_s = \pm 1/2, \pm 1, 0$ values in one oxygen molecule, regardless of the spin distribution of the rest of the electrons in the other three molecules of the molecular oxygen tetramer. At the limit of dissociation, only three possibilities exist, 0, 1, and −1, with equal probabilities (1/3), which is consistent with the formation of a $(O_2)_4$ singlet unit from four O_2 (molecules) triplets. Notice how these two probabilities, the integer projections, are more or less stationary until around d = 2.5 Å, where they diverge, indicating very clearly a change in the magnetic behavior of the $(O_2)_4$ unit. As this critical d value is overcome, the $M_s = \pm 1$ component falls steeply, the $M_s = 0$ one grows to reach a value of 0.35 at 1.5 Å, and the $M_s = \pm 1/2$ component rises very quickly to about 0.25. For this reason, we see how a magnetic collapse cannot be invoked as

dx.doi.org/10.1021/ct301070f | J. Chem. Theory Comput. XXXX, XXX, XXX−XXX

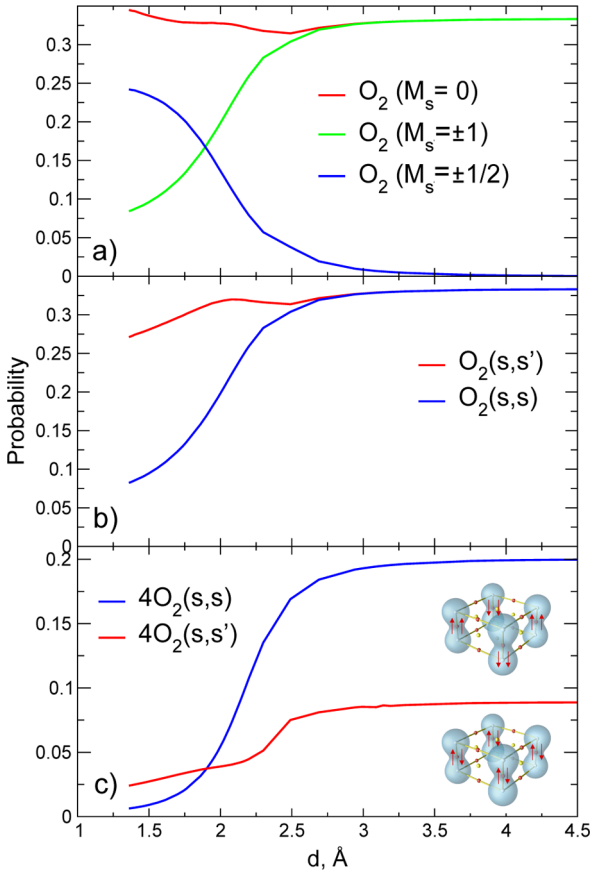

Figure 7. Spin-resolved EDFs for the molecular oxygen tetramer along the compression process. (a) EDF for a M_s component (SM_s), in a given oxygen molecule of the molecular oxygen tetramer. (b) EDF probabilities for a given oxygen molecule within the molecular oxygen tetramer but for unpaired electrons $(s,s) = \alpha\alpha,\beta\beta$ or paired electrons $(s,s') = \alpha\beta$. (c) Same as before but for any oxygen molecule within the tetramer.

an isolated event from the chemical interaction process. It involves a rising probability of finding an odd number of electrons in each molecule, a direct consequence of the exchange mechanism previously described.

Analogously, in Figure 7b, we present the probability $p_{\alpha\alpha}$ of finding two (and exactly two) unpaired electrons and the probability $p_{\alpha\beta}$ of finding two (and exactly two) paired electrons within one of the oxygen molecules, irrespective of the location and spin of the six remaining electrons. At the dissociation limit, both structures have the same probability, but as we compress the molecular oxygen tetramer the behavior of the two curves diverges. $p_{\alpha\alpha}$ displays a sigmoidal behavior upon compression, approaching an asymptotic value equal to 1/3 at dissociation, decreasing to about 0.10 at d = 1.5 Å. On the contrary, $p_{\alpha\beta}$ suffers a drastic modification at about d = 2.5 Å, reaching a minimum, increasing up to d = 2.1 Å, then decreasing again to about 0.27 at the minimum distance reached in the simulation. Noticeably, $p_{\alpha\beta} > p_{\alpha\alpha}$ at distances smaller than 2.5 Å, the difference between both possibilities increasing the larger the compression is. It is important to recall that an overall decrease of the probabilities displayed in Figure 7b is a necessary result from the increase in the intermolecular electron exchange discussed at the end of the last subsection (see the n = 2 curve in Figure 6). In other words, superimposed to the drastic change of the spin structure of the n = 2 case of each oxygen molecule we have the symmetric exchange of one (even two) pairs of electrons among different molecules. This process increases the number of RSRSs that effectively contribute to the EDF, thus decreasing the contribution of the asymptotically dominating n = 2 term. Taking this effect into account, the peculiar behavior of $p_{\alpha\beta}$ with distance stands out.

Finally, we have collected in Figure 7c the probability profiles of the jointly unpaired (s,s) and paired (s,s') resonance structures in the molecular oxygen tetramer. At distances between 1.5 and 1.8 Å the most probable resonance structure is the paired configuration. A crossing occurs at 1.8 Å, and from that point on, the unpaired structure dominates. Notice again a sudden change in the paired term at about d = 2.5 Å which we associate with the onset of the change in magnetic behavior.

All these results show how an intratetramer process starting at d = 2.5 Å destroys the antiferromagnetic coupling predominant in the dissociation region. Thus, although cooperative effects will surely determine the specific point at which this transition is found in the actual solid, we have shown here in sufficient detail that magnetic collapse in ε-O_2 is the result of a spin redistribution within each single molecular oxygen tetramer.

5. CONCLUSIONS

An examination of the intermolecular interactions present in the molecular oxygen tetramer and its evolution from geometries close to those found in the ε phase of solid oxygen to the limit of four monomers shows that, as the cluster is compressed, a noticeable exchange-correlation term appears among nearest neighbor O_2 molecules. These terms are interestingly built from a simultaneous weakening of the intramolecular O−O double bond that, however, almost maintains an O_2 molecular character. These results clearly show that, as generally predicted in the high pressure physics of molecular solids, compression of the molecular oxygen tetramer leads to strengthened intermolecular bonds at the expense of the intramolecular links that account for gas phase molecular structures. In the case examined here, the new interactions cannot be distinguished from incipient covalent bonds. All the topological descriptors and analysis carried out point to the same direction; that is, a partially covalent bond is present in $(O_2)_4$, an interaction that is fundamental for the stabilization of the ε phase of solid oxygen. The concomitant weakening of the O−O intramolecular bond may be at the core of the anomalous behavior of the IR vibron found around 20 GPa, one of the unsolved issues in the δ−ε phase transition.

Intermolecular interactions are crucial for the spin structure of the molecular oxygen tetramer, as evidenced through our Electron population Distribution Functions (EDF). Our results show that along the compression process, two completely different magnetic regions appear. At large intermolecular distances, the four molecules $O_2(^3\Sigma_g^-)$ are arranged in a way compatible with antiferromagnetic coupling. At shorter distances (d < 2.5 Å), exchange drives a spin redistribution where the probability for spin projection M_s = 1 significantly decreases while the M_s = 0 component increases.

Additional calculations of excited electronic states reported here confirm that the monomers of the $(O_2)_4$ cluster do not borrow the character of the low-lying excited singlet states ($^1\Delta_g$ or $^1\Sigma_g^+$) of the isolated molecules. In summary, the origin of the diamagnetic behavior in ε-O_2 should be addressed at the onset of the new intermolecular bonds in the molecular oxygen tetramer and not in a exclusive modification of the electronic character of the monomers.

dx.doi.org/10.1021/ct301070f | J. Chem. Theory Comput. XXXX, XXX, XXX−XXX

As is observed in Figure 1, the qualitative behavior of CASSCF profile is correct: such an energetic profile agrees with a potential energy surface calculated with a higher level of theory. So, we expect that the conclusions made from our IQA and EDF analysis based on CASSCF wave functions are qualitatively right. For example, in the hypothetical case of the availability of CASPT2's order density matrices, the behavior of such results should not be different from those obtained by CASSCF wave functions.

The present work has shown clear evidence that state of the art real space analysis of chemical interactions may be used to shed light on interesting phenomena occurring in molecular solids. Use of multideterminant wave functions has been essential to achieving a reliable conclusion. Further calculations of this cluster beyond the CASSCF level will be surely more quantitative, but more importantly, cooperative effects will have to be taken into account in future work. We think that larger cluster calculations may well show how large these influences will be.

AUTHOR INFORMATION

Corresponding Author

*E-mail: magarcia@ugto.mx.

Author Contributions

⊥The present contribution was done during a postdoctoral possition of M.A.G.-R. at Departamento de Química Física y Analítica, Universidad de Oviedo.

Notes

The authors declare no competing financial interest.

ACKNOWLEDGMENTS

The authors acknowledge financial support from the Spanish MICINN, Projects No. CTQ2009-08376, CTQ2009-14596-02-02, CTQ2012-38599-C02, and FIS2010-22064-C02-02; the European Union FEDER funds; the MALTA-Consolider program (CSD2007-00045); and the CONACyT-167921 project.

REFERENCES

(1) Shimizu, K.; Suhara, K.; Ikumo, M.; Eremets, M.; Amaya, K. *Nature* **1998**, *393*, 767−769.
(2) Lundegaard, L. F.; Weck, G.; McMahon, M. I.; Desgreniers, S.; Loubeyre, P. *Nature* **2006**, *443*, 201−204.
(3) Fujihisa, H.; Akahama, Y.; Kawamura, H.; Ohishi, Y.; Shimomura, O.; Yamawaki, H.; Sakashita, M.; Gotoh, Y.; Takeya, S.; Honda, K. *Phys. Rev. Lett.* **2006**, *97*, 085503.
(4) Weck, G.; Desgreniers, S.; Loubeyre, P.; Mezouar, M. *Phys. Rev. Lett.* **2009**, *102*, 255503.
(5) Sun, J.; Martinez-Canales, M.; Klug, D. D.; Pickard, C. J.; Needs, R. J. *Phys. Rev. Lett.* **2012**, *108*, 045503.
(6) Meng, Y.; Eng, P. J.; Tse, J. S.; Shaw, D. M.; Hu, M. Y.; Shu, J.; Gramsch, S. A.; Kao, C.-c.; Hemley, R. J.; Mao, H.-k. *Proc. Natl. Acad. Sci. U. S. A.* **2008**, *105*, 11640−11644.
(7) Young, D. *Phase Diagrams of the Elements*; University of California Press: Berkeley, CA, 1991.
(8) Freiman, Y.; Jodl, H. *Phys. Rep.* **2004**, *401*, 1−228.
(9) Santoro, M.; Gorelli, F. A.; Ulivi, L.; Bini, R.; Jodl, H. J. *Phys. Rev. B* **2001**, *64*, 064428.
(10) Klotz, S.; Strässle, T.; Cornelius, A. L.; Philippe, J.; Hansen, T. *Phys. Rev. Lett.* **2010**, *104*, 115501.
(11) Akahama, Y.; Kawamura, H. *Phys. Rev. B* **1996**, *54*, 15602.
(12) Gorelli, F. A.; Ulivi, L.; Santoro, M.; Bini, R. *Phys. Rev. B* **2001**, *63*, 104110.
(13) Nicol, M.; Syassen, K. *Phys. Rev. B* **1983**, *28*, 1201−1206.
(14) Goncharenko, I. N. *Phys. Rev. Lett.* **2005**, *94*, 1−4.
(15) Politzer, P.; Lane, P. *Int. J. Quantum Chem.* **2000**, *77*, 336−340.
(16) Neaton, J. B.; Ashcroft, N. W. *Phys. Rev. Lett.* **2002**, *88*, 205503.
(17) Militzer, B.; Hemley, R. J. *Nature* **2006**, *443*, 150−151.
(18) Ma, Y.; Oganov, A. R.; Glass, C. W. *Phys. Rev. B* **2007**, *76*, 064101.
(19) Bartolomei, M.; Carmona-Novillo, E.; Hernández, M. I.; Pérez-Ríos, J.; Campos-Martínez, J.; Hernández-Lamoneda, R. *Phys. Rev. B* **2011**, *84*, 092105.
(20) Bader, R. F. W. *Atoms in Molecules*; Oxford University Press: New York, 1990.
(21) Becke, A. D.; Edgecombe, K. E. *J. Chem. Phys.* **1990**, *92*, 5397−5403.
(22) Savin, A.; Nesper, R.; Wengert, S.; Fassler, T. F. *Angew. Chem., Int. Ed. Engl.* **1997**, *36*, 1809−1832.
(23) Silvi, B.; Savin, A. *Nature* **1994**, *371*, 683−686.
(24) Becke, A. D. *J. Chem. Phys.* **1988**, *88*, 2547−53.
(25) Hirshfeld, F. L. *Theor. Chim. Acta* **1977**, *44*, 129−138.
(26) Fernández Rico, J.; López, R.; Ema, I.; Ludeña, E. *J. Comput. Chem.* **2004**, *25*, 1355−1363.
(27) Cioslowski, J.; Mixon, S. T. *J. Am. Chem. Soc.* **1992**, *114*, 4382−4387.
(28) Haaland, A.; Shorokhov, D. J.; Tverdova, N. V. *Chem.—Eur. J.* **2004**, *10*, 4416−4421.
(29) Farrugia, L. J.; Evans, C.; Tegel, M. *J. Phys. Chem. A* **2006**, *110*, 7952−7961.
(30) Bader, R. F. W.; Fang, D.-C. *J. Chem. Theory Comput.* **2005**, *1*, 403−414.
(31) Poater, J.; Solà, M.; Bickelhaupt, F. M. *Chem.—Eur. J.* **2006**, *12*, 2889−2985.
(32) Poater, J.; Solà, M.; Bickelhaupt, F. M. *Chem.—Eur. J.* **2006**, *12*, 2902−2905.
(33) Bader, R. F. W. *Chem.—Eur. J.* **2006**, *12*, 2896−2901.
(34) Poater, J.; Visser, R.; Solà, M.; Bickelhaupt, F. M. *J. Org. Chem.* **2007**, *72*, 1134−1142.
(35) Grimme, S.; Mück-Lichtenfeld, C.; Erker, G.; Kehr, G.; Wang, H.; Beckers, H.; Willner, H. *Angew. Chem., Int. Ed.* **2009**, *48*, 2592−2595.
(36) Henn, J.; Leusser, D.; Stalke, D. *J. Comput. Chem.* **2007**, *28*, 2317−2324.
(37) Martín Pendás, A.; Francisco, E.; Blanco, M. A.; Gatti, C. *Chem.—Eur. J.* **2007**, *13*, 9362−9371.
(38) García-Revilla, M.; Popelier, P. L. A.; Francisco, E.; Martn Pendaás, A. *J. Chem. Theory Comput.* **2011**, *7*, 1704−1711.
(39) Bader, R. F. W.; Slee, T. S.; Cremer, D.; Kraka, E. *J. Am. Chem. Soc.* **1983**, *105*, 5061−5068.
(40) García-Revilla, M.; Hernandez-Trujillo, J. *Phys. Chem. Chem. Phys.* **2009**, *11*, 8425−8432.
(41) Bader, R. F. W.; Stephens, M. E. *J. Am. Chem. Soc.* **1975**, *97*, 7391−7399.
(42) Fradera, X.; Austen, M. A.; Bader, R. F. W. *J. Phys. Chem. A* **1999**, *103*, 304−314.
(43) Martín Pendás, A.; Francisco, E.; Blanco, M. A. *J. Comput. Chem.* **2005**, *26*, 344−351.
(44) Francisco, E.; Martín Pendás, A.; Blanco, M. A. *J. Chem. Theory Comput.* **2006**, *2*, 90−102.
(45) Martín Pendás, A.; Blanco, M. A.; Francisco, E. *J. Comput. Chem.* **2007**, *28*, 161−184.
(46) Blanco, M. A.; Martín Pendás, A.; Francisco, E. *J. Chem. Theory Comput.* **2005**, *1*, 1096−1109.
(47) Li, L.; Parr, R. G. *J. Chem. Phys.* **1986**, *84*, 1704−17011.
(48) Martín Pendás, A.; Blanco, M. A.; Francisco, E. *J. Chem. Phys.* **2006**, *125*, 184112.
(49) Martín Pendás, A.; Blanco, M. A.; Francisco, E. *J. Comput. Chem.* **2009**, *30*, 98−109.
(50) Tiana, D.; Francisco, E.; Blanco, M. A.; Macchi, P.; Sironi, A.; Pendás, A. M. *Phys. Chem. Chem. Phys.* **2011**, *13*, 5068−5077.
(51) Francisco, E.; Martín Pendás, A.; Blanco, M. A. *J. Chem. Phys.* **2007**, *126*, 094102.
(52) Martín Pendás, A.; Francisco, E.; Blanco, M. A. *J. Chem. Phys.* **2007**, *127*, 144103.

(53) Martín Pendás, A.; Francisco, E.; Blanco, M. A. *Phys. Chem. Chem. Phys.* **2007**, *9*, 1087−1092.
(54) Francisco, E.; Martín Pendás, A.; Blanco, M. A. *Comput. Phys. Commun.* **2008**, *178*, 621−634.
(55) Francisco, E.; Martín Pendás, A.; Blanco, M. A. *J. Chem. Phys.* **2009**, *131*, 124125.
(56) Francisco, E.; Pendás, A. M.; Costales, A.; García-Revilla, M. *Comput. Theor. Chem.* **2011**, *975*, 2−8 . Electronic Structure: Principles and Applications. From basic theory. The 7th Congress on Electronic Structure: Principles and Applications (ESPA-2010).
(57) Huber, K. P.; Herzberg, G. *Molecular Spectra and Molecular Structure: IV. Constants of Diatomic Molecules*; Van Nostrand Reinhold Company: New York, 1979.
(58) Boys, S. F.; Bernardi, F. *Mol. Phys.* **1970**, *19*, 553.
(59) Van Lenthe, J. H.; Duijneveldt-Van Devan Rijdt, J. G. C. M.; Van Duijneveldt, F. B. *Advances in Chemical Physics*; John Wiley & Sons, Inc.: New York, 2007; pp 521−566.
(60) Werner, H.-J.; Knowles, P. J.; Lindh, R.; Manby, F. R.; Schutz, M.; Celani, P.; Korona, T.; Rauhut, G.; Amos, R. D.; Bernhardsson, A.; Berning, A.; Cooper, D. L.; Deegan, M. J. O.; Dobbyn, A. J.; Eckert, F.; Hampel, C.; Hetzer, G.; Lloyd, A. W.; McNicholas, S. J.; Meyer, W.; Mura, M. E.; Nicklass, A.; Palmieri, P.; Pitzer, R.; Schumann, U.; Stoll, H.; Stone, A. J.; Tarroni, R.; Thorsteinsson, T. *MOLPRO*, version 2006.1; Institut für Theoretische Chemie, Universität Stuttgart: Stuttgart, Germany, 2006. see http://www.molpro.net/.
(61) Schmidt, M. W.; Baldridge, K. K.; Boatz, J. A.; Elbert, S. T.; Gordon, M. S.; Jensen, J. H.; Koseki, S.; Matsunaga, N.; Nguyen, K. A.; Su, S. J.; Windus, T. L.; Dupuis, M.; Montgomery, J. A. *J. Comput. Chem.* **1993**, *14*, 1347−1363.
(62) Martín Pendás, A. PROMOLDEN, a QTAIM/IQA code (unpublished).
(63) Keith, T. A.; Laidig, K. E.; Krug, P.; Cheeseman, J. R.; Bone, R. G. A.; Biegler-König, F. W.; Duke, J. A.; Tang, T.; Bader, R. F. W. The AIMPAC95 programs. Avalaible at http://www.chemistry.mcmaster.ca/aimpac.
(64) Steudel, R.; Wong, M. *Angew. Chem., Int. Ed.* **2007**, *46*, 1768−1771.